

Coordination control of distributed generators and load resources for frequency restoration in isolated urban microgrids

Hongxun Hui^b, Yulin Chen^{c,b,*}, Shaohua Yang^b, Hongcai Zhang^b, Tao Jiang^a

^a Key Laboratory of Modern Power System Simulation and Control & Renewable Energy Technology, Ministry of Education (Northeast Electric Power University), Jilin, 132012, China

^b State Key Laboratory of Internet of Things for Smart City, University of Macau, 999078, Macao Special Administrative Region of China

^c Hainan Institute of Zhejiang University, Sanya, 572000, China

ARTICLE INFO

Keywords:

Isolated microgrid
Coordination control
Distributed generator
Flexible loads
Virtual power plants

ABSTRACT

Urban microgrids have become the main body of energy consumption in modern power systems. To reduce carbon emissions, distributed generators (DGs), such as roof photovoltaics (PVs), are increasing rapidly in urban microgrids. By utilizing the power output from local DGs, more microgrids have the ability to operate in isolated mode. However, isolated microgrids have less regulation capacities compared with large interconnected power systems, which significantly raises the difficulty for maintaining the stable operation of isolated microgrids. To address this issue, this paper proposes a coordination control method to tap flexibility from both DGs in supply-side and load resources in demand-side. First, the microgrid model with high-penetration DGs is developed considering virtual power plants (VPPs) by aggregating flexible loads. Then, a coordination control framework is proposed for DGs and VPPs in multi-scenarios, including stable operation, uncertain load disturbances, and accidental DG outages. Based on this framework, a distributed consensus algorithm (DCA) and a local control algorithm (LCA) are designed for DGs and VPPs, respectively. The DCA can achieve a quick regulation of DGs with high plug-and-play expansibility. The LCA can control VPPs considering both the quality of regulation services and comfortable requirements of heterogeneous users. Finally, numerical studies verify that the proposed models and methods can awaken fragmented DGs and VPPs to improve the stability and enhance the resilience of isolated microgrids.

1. Introduction

Urban areas consume about 75% of global primary energy and produce about 80% carbon emissions [1]. Urban microgrids have also become the main body of energy consumption in modern power systems. To reduce carbon emissions in urban areas, renewable distributed generators (DGs) are increasing rapidly. For example, photovoltaics (PVs) have increased around forty times in the past ten years [2]. With the further increase of DGs, microgrids have the ability to operate in the isolated mode, i.e., disconnect with the main grid [3]. However, isolated microgrids have less regulation capacities compared with large interconnected power systems, which significantly raises the difficulty for maintaining the stable operation of isolated microgrids.

To improve the resilience of isolated microgrids, more attentions are paid to local flexible resources. For example, Zheng et al. [4] design a central control scheme for distributed electricity storages in microgrids, which can decrease the microgrids' stress while increasing users' economic benefits. Wang et al. [5] propose an optimal allocation

method for distributed energy storage devices to mitigate the unbalance in microgrids. Zhou et al. [6] present a two-stage load shedding scheme to cope with potential power deficits in isolated microgrids. Hui et al. [7] design a real-time local electricity market for DGs and loads in microgrids to improve the utilization rate of DGs' fluctuating output power. Yan et al. [8] develop a two-level network-constrained peer-to-peer transactive energy framework for utilizing the flexibility of multi-microgrids. However, the above studies mainly focus on utilizing the flexibility from energy storage devices or load shedding, which may increase the operation cost of microgrids and decrease users' comforts in energy consumption.

With the progress of Internet of Things technologies, more load resources can be flexibly regulated while not impacting users' comforts [9]. For example, Shi et al. [10] propose a control strategy to regulate thermostatic loads for providing primary and secondary frequency regulation services within the users' required temperature

* Corresponding author at: State Key Laboratory of Internet of Things for Smart City, University of Macau, 999078, Macao Special Administrative Region of China.

E-mail address: yulinchen@um.edu.mo (Y. Chen).

<https://doi.org/10.1016/j.apenergy.2022.120116>

Received 14 March 2022; Received in revised form 27 August 2022; Accepted 5 October 2022

0306-2619/© 2022 Elsevier Ltd. All rights reserved.

ranges. Hu et al. [11] develop a voltage regulation method for electric vehicles to realize the reactive response without violating their normal active charging demands. Utilizing these inherent load resources in microgrids can avoid the significant increase of cost compared with installing energy storage devices [12]. Specifically, this paper takes air conditioners (ACs) as typical flexible loads to achieve the coordinate control with DGs [13], because ACs account for around 50% of the total urban power consumption and have huge regulation potential [14]. Furthermore, users' requirements on comfortable indoor temperatures can be guaranteed during ACs' regulation process by using buildings' thermal inertia characteristics [15]. Many demonstration projects are carrying out around the world. For example, from 2016 to 2020, a project "Friendly Interactive System of Supply and Demand Sides" was implemented in Jiangsu, China, to decrease the load peak–valley difference [16]. In Aug. 2022, demand response was carried out in Chongqing, China, to regulate ACs in commercial buildings for increasing the energy efficiency. Besides, smart kits are provided to customers in New York, America, for achieving the remote control of ACs and participating in regulation services.

However, the coordination control of massive dispersed DGs and ACs is a trick problem. There are mainly three obstacles, as following:

(1) *Massive individuals*: The regulation capacity of each DG and AC is small (e.g., one DG and one AC may only have 10 kW and 1 kW available regulation capacities, respectively) [17]. To provide significant regulation services for the system, large-scale dispersed DGs and ACs should be aggregated and controlled coordinately [18]. However, DGs and ACs have heterogeneous operating characteristics, e.g., DGs have different installed capacities and power output features [19]. ACs have different rated power, set temperatures, and energy efficiency ratios (EERs), which are installed in buildings with different sizes and thermal resistances [20]. Therefore, the proposed control method should deal with massive DGs and ACs considering heterogeneous regulation characteristics.

(2) *High uncertainties*: Compared with traditional generating units (e.g., thermal and gas power generators), the power output of DGs can be significantly impacted by changeable weather conditions [21]. For example, the power output of PVs has lots of fluctuations due to moving clouds and dynamic radiation intensities. Furthermore, the power consumption of ACs can be significantly impacted by humans, who have many stochastic behaviors [22]. In addition, microgrids also have multiple unstable sources, such as load disturbances and DG outages on different branches [23]. Therefore, the proposed control method should regulate DGs and ACs with highly uncertain states and under multiple accidental operation scenarios.

(3) *Instantaneous control*: Compared with large interconnected power systems, microgrids can be impacted by disturbances more easily due to their less regulation capacities [24]. Furthermore, disturbances can cause a faster impact on microgrids due to their smaller damping features [25]. For example, the frequency drooping period from the beginning of disturbances to the maximum deviation value is generally around 10 s in large power systems while it may be less than 1s in microgrids [26]. That is to say, massive dispersed DGs and ACs should be optimized and controlled in a very short time. Therefore, a quick solution algorithm should be designed to combine with the proposed control method oriented to both DGs and ACs.

Faced with the above difficulties, Shi et al. [27] propose a resilience-oriented DG siting and sizing method considering stochastic scenarios. However, this paper only pays attention to fuel-based thermal generators while not renewable energies with higher uncertainties (e.g., PVs). ACs are equivalent to generating units in [28] and thermal batteries in [29] to provide regulation services for power systems, respectively. However, these studies are carried out in large power systems while not isolated microgrids. An edge-cloud integrated solution [30] and a deep reinforcement learning method [31] are proposed for regulating building-level loads, while these methods are only tested by a few individuals and may be insufficient for large-scale ACs. A fast

distributionally robust chance-constrained dispatch method [32] and a scenario-based stochastic nonconvex mixed integer nonlinear programming method [33] are proposed to regulate the energy consumption of ACs, while these studies are done for the day-ahead optimization without considering the real-time fast control of ACs [34]. In summary, to the best of our knowledge, there is no specific study on the coordination control of DGs and ACs in isolated microgrids.

To address the aforementioned issues, this paper proposes a coordination control method to tap flexibility from both DGs in supply-side and ACs in demand-side. The main contributions are summarized as follows:

(1) The isolated microgrid model is developed considering high-penetration renewable DGs and massive adjustable ACs, where heterogeneous ACs are aggregated as virtual power plants (VPPs) to provide regulation services for the microgrid [35]. On this basis, a coordination control framework is designed for DGs and VPPs in multi-scenarios, including stable operation, uncertain load disturbances, and accidental DG outages.

(2) A distributed consensus algorithm (DCA) is designed for DGs under the coordination control framework. Compared with traditional centralized control algorithms, the DCA can achieve a quick regulation of DGs with low communication requirement while good plug-and-play expansibility to deal with highly uncertain DGs.

(3) A local control algorithm (LCA) is designed for ACs in each VPP, which regulates ACs based on terminal detecting data to avoid real-time communication and increase the control speed. The LCA can fulfill the quality of regulation services for microgrids without compromising heterogeneous users' comfortable requirements.

The remainder of this paper is organized as follows. Section 2 presents the coordination control framework for DGs and VPPs. Section 3 shows the modeling and DCA control methods for DGs. Section 4 formulates the thermal–electrical model of ACs and aggregates them as VPPs to provide regulation services. Numerical studies and results are presented in Section 5. Finally, Section 6 concludes this paper.

2. Coordination control framework

2.1. Modeling of the microgrid

Fig. 1 shows a microgrid with DGs and VPPs, which can operate in both isolated and grid-connected modes [36]. When the microgrid operates in grid-connected mode, its frequency and voltage are dictated by the main grid [37]. In this condition, DGs in the microgrid are generally operated with the maximum power point tracking control mode to facilitate the utilization of renewable energies [38]. However, when the microgrid switches to the isolated mode due to the preplanned scheduling or unexpected accidental disconnection, the frequency and voltage stability should be maintained by local DGs and VPPs. In the supply-side in Fig. 1, distributed PVs are considered as DGs to provide power output to the microgrid. In the demand-side, the power is consumed by two kinds of loads, i.e., adjustable ACs and other fixed loads. The adjustable ACs on each bus are aggregated as a VPP to provide regulation services for the microgrid. The fixed loads refer to loads whose power consumption is decided by users and cannot be controlled to provide regulation services.

In the microgrid, there are two kinds of communication links:

(1) *The first kind* is the external communication for connecting the operator with DGs and VPPs, which transmits the coordination control protocol before the dispatch interval or day-ahead, including the control reference of system frequency ω^* for DGs and the frequency deviation threshold $\Delta\omega_{thr}$ for VPPs. Hence, the external communication does not require real-time and high-speed, which helps to decrease the communication construction cost between the microgrid operator and massive distributed resources. After the regulation, the external communication transmits the regulation results of DGs and VPPs (e.g., the

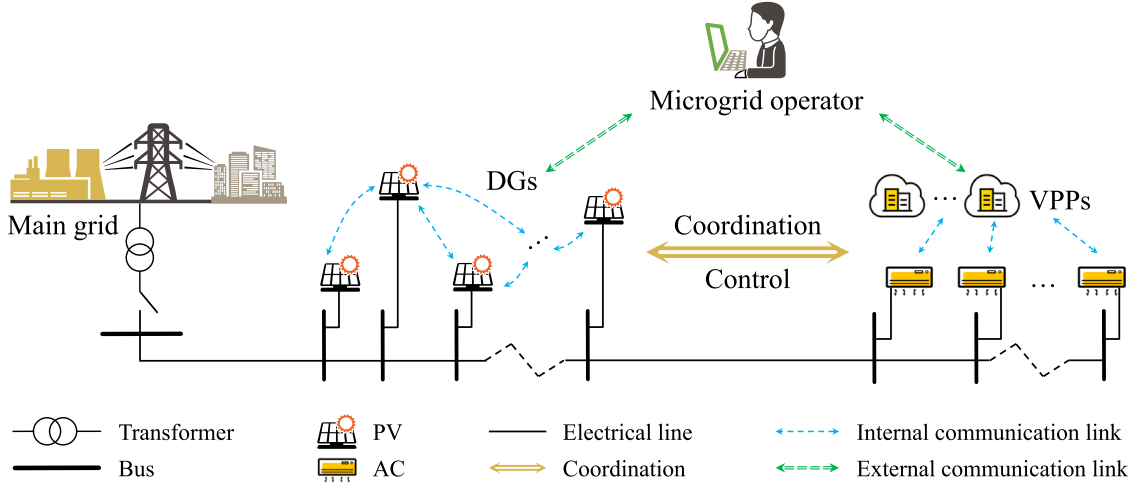


Fig. 1. The coordination control framework of DGs and VPPs in a microgrid.

provided capacities and duration time) to the microgrid operator for the final settlement.

(2) *The second kind* is the internal communication among DGs and within VPPs. The internal communication among DGs can connect different devices to achieve the DCA. Each DG mainly connects with its neighbor devices, which contributes to decreasing the communication distance. Compared with the external communication, the internal communication requires the real-time function to transmit local regulation data among DGs, including the angular frequency ω_i and active power P_i . Another internal communication is for the VPP to connect with its corresponding ACs to achieve the LCA. The transmitted information is the frequency deviation threshold $\Delta\omega_{thr}$. Generally, ACs in a building or a community are aggregated as a VPP. Thus, the internal communication for ACs is also with short distance. The specific control algorithms (i.e., DCA for DGs and LCA for ACs) will be illustrated in Sections 3 and 4, respectively.

2.2. Coordination control protocol of DGs and VPPs

Considering multiple operation scenarios (e.g., stable operation with small disturbances, accidental large disturbances, and serious DG outages), the coordination control protocol is designed by the following principle: making full use of DGs first and then utilizing VPPs to assist the microgrid's balance in some serious conditions. That is to say, no matter in which scenario, DGs are connected into the microgrid to provide regulation services. By contrast, VPPs in the demand-side do not provide regulation services in relatively stable operation states (e.g., the system frequency deviation is less than 0.1 Hz). VPPs only start to participate in the regulation in some larger disturbances (e.g., the system frequency deviation is larger than 0.1 Hz) or some serious DG outages (e.g., the system frequency plunges abruptly and deviation reaches 0.3 Hz) [39]. The proposed coordination manner can avoid to control VPPs frequently, which can reduce the impacts on users' energy consumption, especially considering microgrids operate in a relatively stable state most of time.

As for DGs in the microgrids, each one plays an equal role to support the stable operation of the microgrid [40]. The fair utilization profile method is employed to regulate DGs [41], which can be expressed as:

$$\frac{P_1}{P_1^{\max}} = \frac{P_2}{P_2^{\max}} = \dots = \frac{P_N}{P_N^{\max}}, \quad (1)$$

where $i = 1, 2, \dots, N$ indicates the number of DGs. Symbols P_i and P_i^{\max} are the real-time actual power output and the maximum available power output of the i th DG, respectively. That is to say, the reference value for the fair utilization profile method is the real-time available power output of each DG, which is dynamic with time.

3. Modeling and control of DGs

3.1. Modeling of DGs

DGs in this paper are considered as PV systems, which can be modeled as inverter-based voltage sources with photovoltaic panels. Fig. 2 shows the block diagram of an inverter-based DG. The photovoltaic panel connects to the microgrid through a direct-current/alternating-current inverter, a LC filter¹ and a output connector. The local control of the DG includes an inner current controller, an inner voltage controller, and a PWM controller in a cascade configuration [42]. The inner current and voltage controllers get regulation references from the primary controller, which can be designed to regulate the inverter-based DG and will be introduced in details.

For maintaining the microgrid balance, DGs requires at least two control levels, i.e., the primary control and the secondary control. The primary control is usually implemented by the droop control method, which is a local control method without any communication involved. The basic principle of the droop control is to mimic the operation of traditional synchronous generator, which lies in prescribing a desired relation between the angular frequency ω_i and the active power P_i , and lies in prescribing a desired relation between the voltage amplitude V_i and the reactive power Q_i , respectively. The droop characteristic of the i th DG can be expressed as:

$$\begin{cases} \omega_i = \omega_i^* - m_i P_i, \\ v_i^{dref} = V_i^* - n_i Q_i, \\ v_i^{qref} = 0, \end{cases} \quad (2)$$

where ω_i^* and V_i^* are the control references; m_i and n_i are the droop coefficients and generally determined by the power ratings of corresponding DGs; v_i^{dref} and v_i^{qref} are the references for the inner current controller [36].

Then, the inner current controller can be given according to the references, v_i^{dref} and v_i^{qref} , provided by the primary control as follows [43]:

$$\begin{cases} i_i^{dref} = (K_{P_i}^v + \frac{K_{I_i}^v}{s})(v_i^{dref} - v_i^{od}) - \omega_b C_i^F v_i^{oq} + F_i i_i^{od}, \\ i_i^{qref} = (K_{P_i}^v + \frac{K_{I_i}^v}{s})(v_i^{qref} - v_i^{oq}) + \omega_b C_i^F v_i^{od} + F_i i_i^{oq}, \end{cases} \quad (3)$$

where $K_{P_i}^v$ and $K_{I_i}^v$ are the proportional and integral coefficients of the voltage control loop, respectively; v_i^{od} , v_i^{oq} , i_i^{od} and i_i^{oq} are the

¹ The LC filter refers to the circuit consisting of a combination of inductors (L) and capacitors (C) to cut or pass specific frequency bands of electricity.

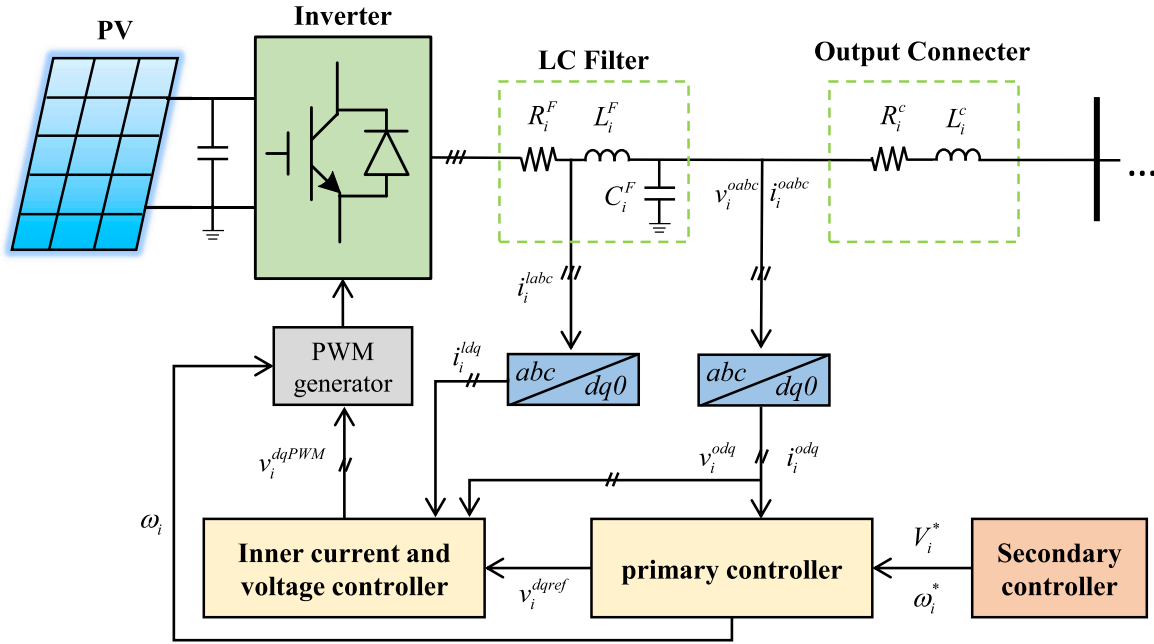


Fig. 2. Block diagram model of an inverter-based DG.

direct and quadrature components of v_i^{abc} and i_i^{abc} in Fig. 2; F_i is the feedforward gain; C_i^F is the capacity of the LC filter; ω_b is the nominal angular frequency. The terms $F_i i_i^{pd}$ and $F_i i_i^{pq}$ are responsible for improving the dynamic performance of the voltage controller under disturbances, while the terms $\omega_b C_i^F v_i^{od}$ and $\omega_b C_i^F v_i^{od}$ can ensure the complete decoupling of the current in the d-q axis.

The inner voltage controller can be given according to the generated references of the current controller i_i^{dref} and i_i^{qref} , which can be expressed by:

$$\begin{cases} v_i^{dPWM} = (K_{P_i}^c + \frac{K_{I_i}^c}{s})(i_i^{dref} - i_i^d) - \omega_b L_i^F i_i^{dq}, \\ v_i^{qPWM} = (K_{P_i}^c + \frac{K_{I_i}^c}{s})(i_i^{qref} - i_i^q) + \omega_b L_i^F i_i^d, \end{cases} \quad (4)$$

where $K_{P_i}^c$ and $K_{I_i}^c$ are the proportional and integral coefficients of the current control loop, respectively; i_i^d and i_i^q are the direct and quadrature components of i_i^{abc} in Fig. 2; L_i^F is the inductance of the LC filter; ω_b is the nominal angular frequency. The generated v_i^{dPWM} and v_i^{qPWM} are the references of the PWM generator.

The primary control uses local detected data and can regulate the DG in a short time frame, which is usually designed as an inherent controller for the DG (i.e., the droop coefficients m_i and n_i). However, the primary control is only able to regulate the frequency and voltage into pre-specified ranges to maintain the basic stable operation of the microgrid. It might cause frequency and voltage deviations from their nominal values (e.g., the frequency nominal value may be 50 Hz and voltage nominal value may be 10 kV). Therefore, the secondary control is designed to regulate the control references ω_i^* and V_i^* to compensate for the deviations caused by the primary control. The secondary control is usually with a longer response time than that of the primary control, which guarantees the decoupled design of these two control processes. This paper proposes a DCA for the secondary control of DGs, which is presented in detail in Section 3.2.

3.2. Control of DGs

The principle of the secondary control is to set the control references ω_i^* and V_i^* in (2) to compensate the frequency and voltage back to their nominal values. Conventionally, the secondary control is implemented by the centralized control frame, as shown in Fig. 3(a). It requires

a control center to collect data from all the DGs, execute decision making and send the decision signals back to each DG. Therefore, a star structure with real-time bidirectional communication is required. However, the centralized structure is potentially unreliable due to the single point of failure, and generally with poor scalability. Alternatively, a distributed control structure is proposed in this paper to overcome the shortcoming of the centralized frame, as shown in Fig. 3(b). The external links are utilized to preset references before the dispatch interval (e.g., the frequency reference ω^*). The internal links are for real-time communication among different local DGs to achieve the distributed control.

The distributed secondary control of DGs can be regarded as a distributed tracking synchronization problem, which is usually realized by the distributed cooperative control of a multi-agent system. In other words, all the DGs try to coordinate their terminal frequencies and voltages to the prespecified reference values utilizing local measurements and neighboring communications [44]. In this paper, for realizing the accurate power sharing among DGs in (1), the DCA is employed to develop distributed cooperative control frame of DGs. Here this paper mainly focuses on the frequency stability of microgrids. Thus the active power sharing problem in the secondary control level will be studied in detail, i.e., providing ω_i^* to the primary controller for regulating the active power P_i and the angular frequency ω_i .

The DCA for each DG is realized by sharing its angular frequency ω_i and active power P_i through a communication network with neighbors, as shown in Fig. 3(b). The network can be represented by a digraph $\mathcal{G} = (\mathcal{V}, \mathcal{E})$, where \mathcal{V} is the set of DGs and \mathcal{E} is the set of communication links ($\mathcal{E} \subset \mathcal{V} \times \mathcal{V}$). An existing communication link $(i, j) \in \mathcal{E}$ means DG i can receive information from DG j , i.e., DG j is the neighbor of DG i . The communication links can be defined by an adjacency matrix $A = [a_{ij}]$ with proper dimensions, where $a_{ij} = 1$ if $(i, j) \in \mathcal{E}$. Otherwise, $a_{ij} = 0$ if $(i, j) \notin \mathcal{E}$. To achieve the microgrid frequency restoration and active power sharing of DGs, differentiating (2) yields:

$$\dot{\omega}_i = \dot{\omega}_i^* - m_i \dot{P}_i. \quad (5)$$

Then, the distributed secondary control (i.e., the adjustment value of angular frequency reference ω_i^*) can be provided by the following

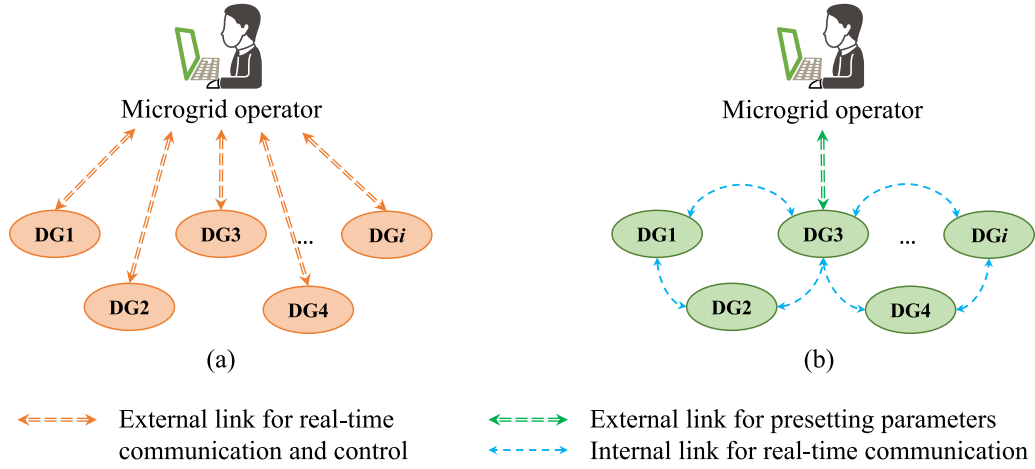


Fig. 3. Control frameworks of DGs: (a) Centralized control; (b) Distributed control.

linear first-order multi-agent system:

$$\begin{cases} \dot{\omega}_1 + m_1 \dot{P}_1 = u_{f p 1}, \\ \dots \\ \dot{\omega}_N + m_N \dot{P}_N = u_{f p N}. \end{cases} \quad (6)$$

where $u_{f p i}$ is another expression of $\dot{\omega}_i^*$ to indicate the adjustment value of angular frequency reference. On this basis, the DCA control law for the i th DG is given by:

$$u_{f p i} = -\kappa_{\omega p} \left[\sum_{j \in \mathcal{N}_i} a_{ij} (\omega_i - \omega_j) + b_i (\omega_i - \omega^r) + \sum_{j \in \mathcal{N}_i} a_{ij} (m_i P_i - m_j P_j) \right], \quad (7)$$

where $\kappa_{\omega p} > 0$ is the coupling gain; ω^r is the rated frequency reference (e.g., 50 Hz); $\mathcal{N}_i = \{j | (i, j) \in \mathcal{E}\}$ is defined as the set of the i th DG's neighbors; b_i is the pinning gain. Symbol $b_i = 1$ indicates the i th DG can receive the rated frequency reference, while $b_i = 0$ indicates the i th DG cannot receive the rated frequency reference.

The two terms in (7) can be combined and reformulated as:

$$\begin{aligned} u_{f p i} &= -\kappa_{\omega p} \left\{ \sum_{j \in \mathcal{N}_i} a_{ij} [(\omega_i + m_i P_i) - (\omega_j + m_j P_j)] + b_i [(\omega_i + m_i P_i) - (\omega^r + m_i P_i)] \right\} \\ &= -\kappa_{\omega p} \left[\sum_{j \in \mathcal{N}_i} a_{ij} (\omega_i^P - \omega_j^P) + b_i (\omega_i^P - \omega^{Pr}) \right], \end{aligned} \quad (8)$$

where $\omega_i^P = \omega_i + m_i P_i$ and $\omega^{Pr} = \omega^r + m_i P_i$, respectively. In this paper, let $m_i = \frac{1}{P_i^{\max}}$ for achieving the fair utilization of each DG.

Based on the $u_{f p i}$ in (8), the angular frequency reference ω_i^* can be calculated by:

$$\omega_i^* = \int u_{f p i} dt. \quad (9)$$

Notice that the fair power sharing mechanism is included in the control law (8). That is to say, both ω_i and $m_i P_i$ can be synchronized by (8). The following lemma provides the synchronization correctness of the proposed DCA secondary control of DGs.

Lemma 1. Consider a microgrid with N DGs connected by a digraph (directed communication network). Let the digraph be a spanning tree and $b_i = 1$ for one DG placed on a root node of the digraph. Each DG is regulated by the control law in (8). Then, all DGs' frequencies ω_i can synchronize to the reference value ω^r . In the meanwhile, the active power provided by each DG P_i can be allocated fairly [45]. Specifically, the two synchronizations can be expressed as:

$$\begin{cases} \lim_{t \rightarrow \infty} |\omega_i - \omega^r| = 0, \\ \lim_{t \rightarrow \infty} |m_i P_i - m_j P_j| = 0. \end{cases} \quad (10)$$

Proof. For the DCA control law in (7), it can be separated into two controllers, i.e., the active power sharing controller and the frequency restoration controller. Combining with (6), the dynamic of the active power sharing controller can be given by:

$$m_i \dot{P}_i = -\kappa_{\omega p} \sum_{j \in \mathcal{N}_i} a_{ij} (m_i P_i - m_j P_j), \quad (11)$$

and the dynamic of the frequency restoration controller can be given by:

$$\dot{\omega}_i = -\kappa_{\omega p} \sum_{j \in \mathcal{N}_i} a_{ij} (\omega_i - \omega_j) - b_i (\omega_i - \omega^r). \quad (12)$$

Thus, Eq. (11) is a consensus algorithm which has been proved to make each agent asymptotically reach consensus [46], i.e., $\lim_{t \rightarrow \infty} |m_i P_i - m_j P_j| = 0$ can be achieved.

Eq. (12) is a leader–follower consensus algorithm, its collective dynamic can be represented as:

$$\dot{\omega} = -\kappa_{\omega p} (L + B) (\omega - \omega^r \mathbf{1}_n), \quad (13)$$

where $\omega = [\omega_1, \omega_2, \dots, \omega_n]^T$; L is the Laplacian matrix, whose elements are defined by $l_{ii} = \sum_{j=1}^n a_{ij}$ and $l_{ij} = -a_{ij}$ ($i \neq j$); $B = \text{diag}\{[b_1, b_2, \dots, b_n]^T\}$ is the pinning matrix; $\mathbf{1}_n$ is a vector with all elements being equal to 1.

Applying Laplace transform to (13), we have the following equation:

$$s\omega(s) - \omega(0) = -\kappa_{\omega p} (L + B) \omega(s) + \frac{\kappa_{\omega p} \omega^r}{s} (L + B) \mathbf{1}_n. \quad (14)$$

Rearranging (14), we can derive:

$$[sI + \kappa_{\omega p} (L + B)] \omega(s) = \omega(0) + \frac{\kappa_{\omega p} \omega^r}{s} (L + B) \mathbf{1}_n. \quad (15)$$

where I is the identity matrix.

Since $(L + B)$ is invertible [47,48], (15) can be derived to:

$$\omega(s) = [sI + \kappa_{\omega p} (L + B)]^{-1} [\omega(0) + \frac{\kappa_{\omega p} \omega^r}{s} (L + B) \mathbf{1}_n]. \quad (16)$$

Applying terminal value theorem to (16), we have:

$$\begin{aligned} \lim_{t \rightarrow \infty} \omega(t) &= \lim_{s \rightarrow 0} s\omega(s) \\ &= \lim_{s \rightarrow 0} [sI + \kappa_{\omega p} (L + B)]^{-1} [s\omega(0) + \kappa_{\omega p} \omega^r (L + B) \mathbf{1}_n] \\ &= \kappa_{\omega p}^{-1} (L + B)^{-1} \kappa_{\omega p} \omega^r (L + B) \mathbf{1}_n \\ &= \omega^r \mathbf{1}_n. \end{aligned} \quad (17)$$

which implies $\lim_{t \rightarrow \infty} |\omega_i - \omega^r| = 0$.

Therefore, we can conclude that all the DGs' frequencies ω_i can synchronize to the reference value ω^r . In the meanwhile, the active power provided by each DG P_i can be allocated fairly.

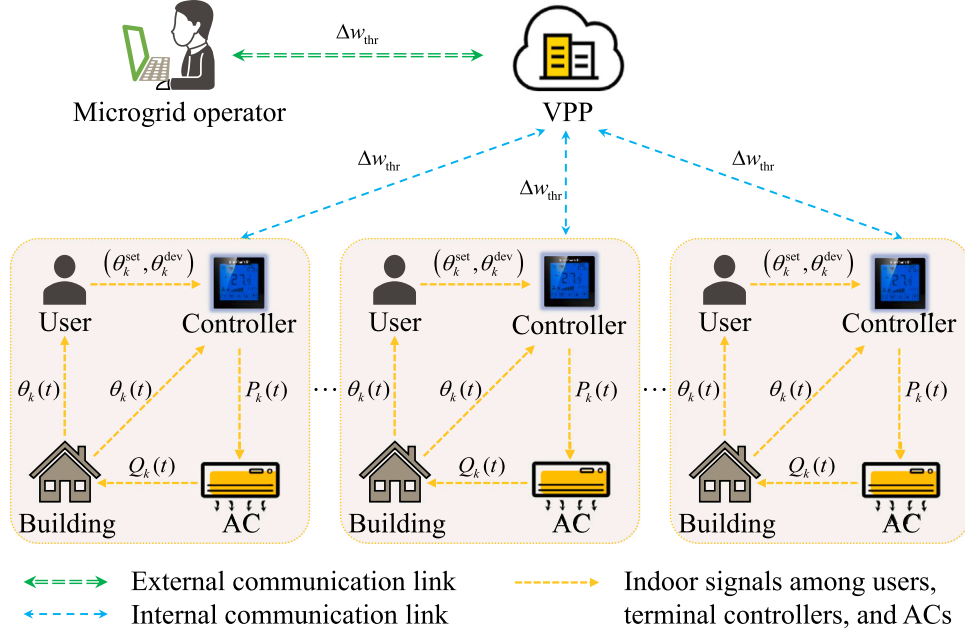


Fig. 4. Control scheme of aggregated ACs as VPP for providing regulation services in microgrid [49].

4. Modeling and control of VPPs

4.1. Modeling of ACs

The VPP in this paper is consist of ACs, because ACs account for around 50% of the total urban microgrid's power consumption and have huge regulation potential. The AC's power consumption is related to the corresponding building's thermal characteristic and ambient temperature. Therefore, this subsection develops the thermal and electrical models for buildings and ACs, as follows [50]:

$$C_k \frac{\partial \theta_k(t)}{\partial t} = \frac{\theta_o(t) - \theta_k(t)}{R_k} - Q_k(t), \quad (18)$$

where $\theta_k(t)$ and $\theta_o(t)$ are the k th building's indoor temperature and the outdoor ambient temperature at time t , respectively; C_k and R_k are the k th building's thermal capacity and the thermal resistance, respectively; Q_k is the k th AC's cooling capacity in the building, which can be calculated as:

$$Q_k(t) = \eta_k P_k(t), \quad (19)$$

where η_k and $P_k(t)$ are the EER and operating power of the k th AC, respectively. Generally, EER distributes among 2.6~3.6, whose cooling efficiency will be higher with a larger EER.

4.2. Control of aggregated ACs as a VPP

If the AC is operating in a stable state and the indoor temperature is equal to the user's set value (i.e., $\theta_k(t) = \theta_k^{\text{set}}(t)$), the $\frac{\partial \theta_k(t)}{\partial t}$ in (18) is equal to 0. Then, the AC's operating power in the stable state can be calculated by:

$$P_k(t) = \frac{\theta_o(t) - \theta_k^{\text{set}}(t)}{\eta_k R_k}. \quad (20)$$

By contrast, if the indoor temperature is not equal to the user's set value (e.g., $\theta_k(t) > \theta_k^{\text{set}}(t)$), the AC will increase its operating power to cool down the indoor temperature [51]. The proportional integral controller is generally utilized and expressed as:

$$\Delta P_k(t) = \epsilon_k (\theta_k(t) - \theta_k^{\text{set}}(t)) + \zeta_k \int (\theta_k(t) - \theta_k^{\text{set}}(t)) dt, \quad (21)$$

where ϵ_k and ζ_k are the proportional and integral factors of the k th AC, respectively. The two factors are set as $\epsilon_k > 0$ and $\zeta_k > 0$ to make sure the $\Delta P_k(t)$ is positive when the actual indoor temperature $\theta_k(t)$ is higher than the set value $\theta_k^{\text{set}}(t)$. In other words, the parameters are set to increase the AC's operating power to generate more cooling capacity when the indoor temperature is too hot.

Fig. 4 shows the control scheme of aggregated ACs as a VPP for supporting the frequency stability of the microgrid [49]. There are three main bodies: the microgrid operator, VPP, and ACs. Before each dispatch interval, the microgrid operator sends the frequency deviation threshold (i.e., $\Delta \omega_{\text{thr}}$) to the VPP, which is then sent to all the terminal controllers of ACs. This threshold $\Delta \omega_{\text{thr}}$ means the VPP begins to provide frequency support when the system frequency deviation is larger than this value.

As for each AC, its operating power P_k is regulated by the corresponding terminal controller, as shown in Fig. 4. Based on (19), the AC generates cooling capacity Q_k to adjust the indoor temperature θ_k . The users in the building can set the desired temperature θ_k^{set} and the maximum allowable deviation ranges θ_k^{dev} to the terminal controller. When the local frequency deviation $\Delta \omega_k$ is smaller than the threshold $\Delta \omega_{\text{thr}}$, the AC is controlled by (21) and does not provide regulation services for the microgrid. By contrast, when the microgrid's frequency deviation $\Delta \omega_k$ is larger than the threshold $\Delta \omega_{\text{thr}}$, the AC will provide regulation services for the microgrid and is controlled as:

$$\Delta P_k(t) = \delta_k (\omega_k(t) - \omega^r) + \gamma_k \int (\omega_k(t) - \omega^r) dt, \quad (22)$$

where ω_k and ω^r are the local detected frequency of the k th AC and the rated frequency reference, respectively. Symbols δ_k and γ_k are the proportional and integral factors of the k th AC for participating in frequency regulation services of the microgrid, respectively. The two factors are set as $\delta_k > 0$ and $\gamma_k > 0$ to make sure the $\Delta P_k(t)$ is negative when the actual microgrid frequency deviation is negative. In other words, if the disturbances lead to the decrease of microgrid frequency, the AC's operating power $\Delta P_k(t)$ will be reduced to support the frequency stability.

Based on each AC's regulation power in (22), the total regulation capacity provided by the VPP can be obtained by:

$$P_{\text{VPP}}(t) = \sum_{k=1}^K S_k(t) \Delta P_k(t). \quad (23)$$

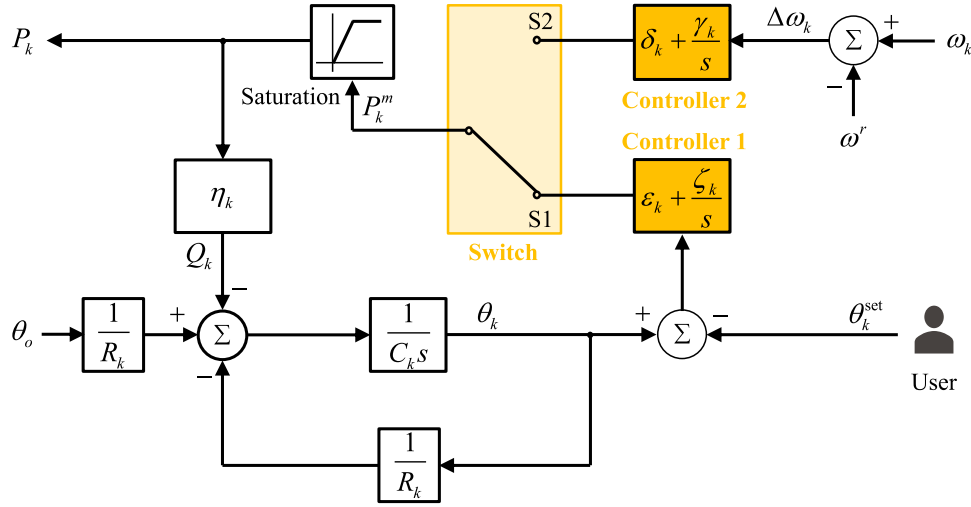


Fig. 5. Control block of an AC for providing regulation services for the microgrid.

Table 1

The algorithm for switching the two controllers.

01	The terminal controller obtains the parameters, including the local detected frequency ω_k , the rated reference frequency ω^r , the frequency deviation threshold $\Delta\omega_{thr}$, the real-time indoor temperature θ_k , the user's set temperature θ_k^{set} , and the user's maximum allowable deviation range of the indoor temperature θ_k^{dev} .
02	If $ \omega_k - \omega^r > \Delta\omega_{thr}$ and $ \theta_k - \theta_k^{set} \leq \theta_k^{dev}$
03	Switch to S2;
04	Else
05	Switch to S1;
06	End

where K is the total number of ACs in this VPP; ΔP_k is the regulation power from the k th AC; S_k is the k th AC's state, i.e., $S_k(t) = 1$ if the AC participates in the regulation service, while $S_k(t) = 0$ if the AC does not participate in the regulation service.

Fig. 5 shows the control block of an AC for providing regulation services for the microgrid. In the complex frequency domain, the thermal model of the building installed with an AC in (18)–(19) can be expressed as:

$$\theta_k(s) = \frac{1}{1 + C_k R_k s} (\theta_o(s) - \eta_k R_k P_k(s)), \quad (24)$$

where s is the Laplace operator.

The saturation block represents the AC's operating power should be constrained as:

$$P_k(s) = \begin{cases} P_k^m, & P_k^m \leq P_k^r, \\ P_k^r, & P_k^m > P_k^r, \end{cases} \quad (25)$$

where P_k^r is the k th AC's rated power, i.e., the maximum operating power.

The two controllers in Fig. 5 are for adjusting the indoor temperature (i.e., Controller 1) and participating in the regulation service (i.e., Controller 2), respectively. The expressions of the two controllers in the time domain in (21)–(22) can be reformulated in the complex frequency domain, as following:

$$\Delta P_k(s) = \begin{cases} (\epsilon_k + \frac{\zeta_k}{s})(\theta_k(s) - \theta_k^{set}(s)), & \text{Switch} = S1, \\ (\delta_k + \frac{\gamma_k}{s})(\omega_k(s) - \omega^r), & \text{Switch} = S2. \end{cases} \quad (26)$$

The algorithm for switching the two controllers are shown in Table 1. When the microgrid's frequency deviation $\Delta\omega_k$ exceeds the threshold $\Delta\omega_{thr}$ and the indoor temperature is in the comfortable range, the switch will be connected to S2 for participating in the regulation service. By contrast, the switch will be connected to S1 and the AC is

only adjusted by the user's set temperature. Furthermore, if the AC is in the regulation service state, there are three conditions to stop the regulation process: (i) the dispatch duration is over (e.g., 15 min); (ii) the actual frequency deviation $\Delta\omega_k$ is decreased to be smaller than the threshold $\Delta\omega_{thr}$; (iii) the indoor temperature $\theta_k(t)$ exceeds the allowable deviation ranges θ_k^{dev} , i.e., $\theta_k(t) \notin [\theta_k^{set} - \theta_k^{dev}, \theta_k^{set} + \theta_k^{dev}]$. In this manner, heterogeneous users' requirements on the indoor temperatures can always be guaranteed.

Fig. 6 shows the whole process of the above coordination control for DGs and VPPs. First, the operator monitors the operating mode of the microgrid and starts the coordination control when the microgrid is in the isolated mode. Before each dispatch interval, the operator transmits the control reference of system frequency ω^r to DGs and the frequency deviation threshold $\Delta\omega_{thr}$ to VPPs. Then, the VPPs transmit the threshold value $\Delta\omega_{thr}$ to ACs in the available regulation state. In the real-time, if accidental events occur, DGs will be controlled fairly by the proposed DCA through transmitting the angular frequency ω_i and active power P_i . VPPs will be controlled by the LCA through detecting the system frequency deviations locally. The regulation capacities from DGs and VPPs are monitored by smart meters for quantifying their regulation profits. Finally, the process enters the next round of dispatch interval if this round of dispatch interval is over.

5. Case study

5.1. Test system

Fig. 7 shows the test system of a 7-bus microgrid with 4 DGs and 3 VPPs. The rated frequency of the microgrid ω^r is 50 Hz. The installed capacities of DGs are as following: $P_1^{max} = 40$ kW, $P_2^{max} = 20$ kW, $P_3^{max} = 40$ kW, and $P_4^{max} = 20$ kW. The parameters of ACs and corresponding buildings are from a realistic demonstration project in China. The living areas of the buildings are among 20~50 m². The thermal capacities C_k and the thermal resistance R_k are among 60~150 kJ/°C and 0.216~0.513 kW/°C, respectively. The rated power P_k^r and the EER η_k of ACs are around 1~2 kW and 2.6~3.6, respectively. The factors for regulating ACs are set as $\epsilon_k = 8.32$ W/°C, $\zeta_k = 0.512$ W/(°C s), $\delta_k = 8$ kW/Hz and $\gamma_k = 0.32$ W/Hz, respectively. It is assumed that each VPP has 10~20 ACs, whose set temperatures θ_k^{set} distribute among 18~27 °C according to heterogeneous users' requirements. The maximum deviation of the indoor temperature θ_k^{dev} is 1 °C. The outdoor temperature θ_o is 35 °C. The regulation duration period is 15 min. The

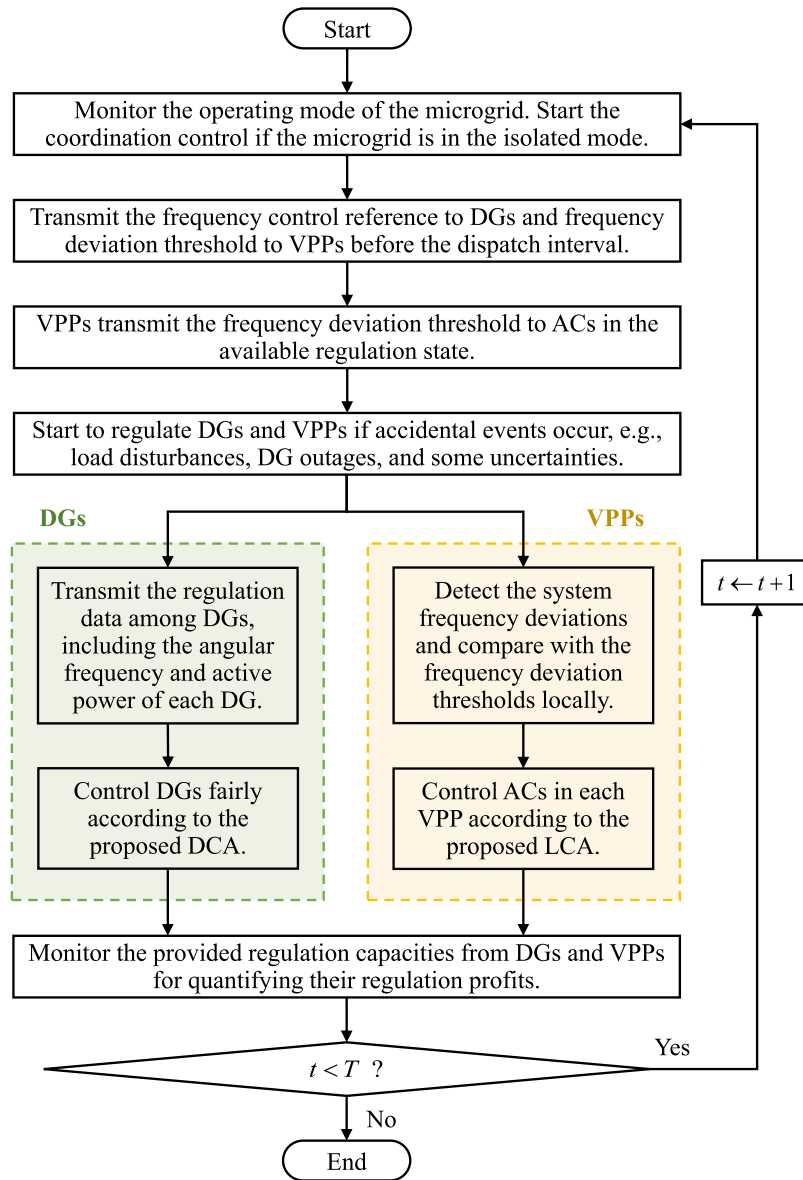


Fig. 6. A flowchart of the coordination control for DGs and VPPs.

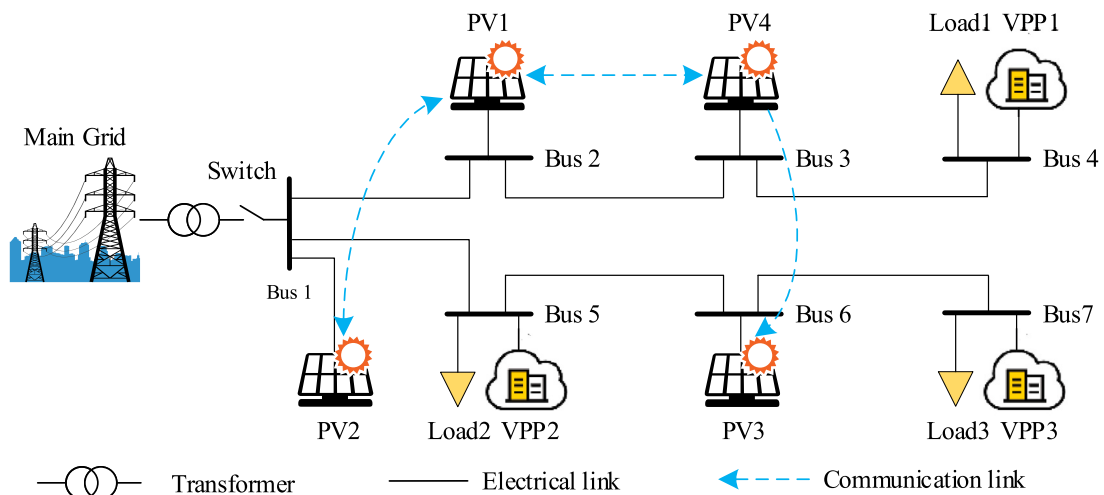


Fig. 7. The test system of a 7-bus microgrid with 4 DGs and 3 VPPs.

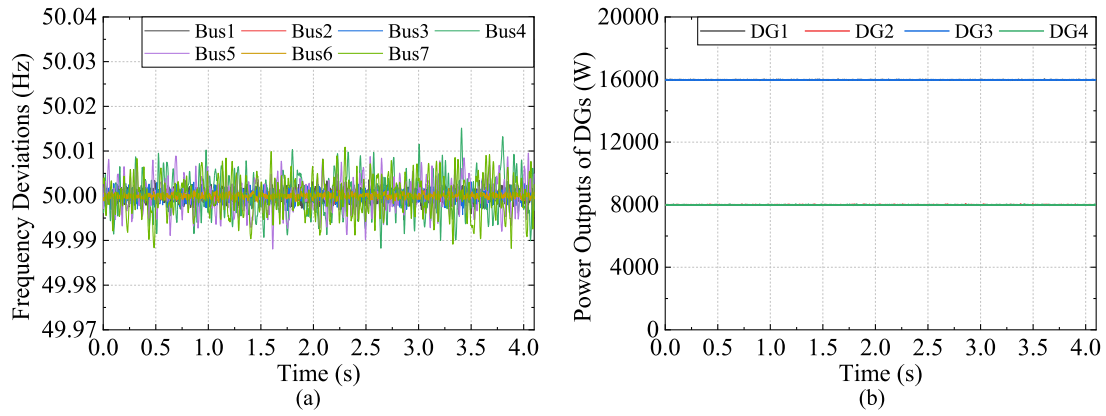


Fig. 8. The initial operating states of the isolated microgrid: (a) the frequency deviations on buses, (b) the generating power outputs of DGs.

frequency deviation threshold for ACs participating in regulation services is set as $\Delta\omega_{thr} = 0.05$ Hz. The pinning gain and the communication links among DGs (i.e., the adjacency matrix A) are as follows:

$$b = \begin{bmatrix} 1 \\ 0 \\ 0 \\ 0 \\ 0 \end{bmatrix}, \quad A = \begin{bmatrix} 0 & 1 & 0 & 1 \\ 1 & 0 & 0 & 0 \\ 0 & 0 & 0 & 1 \\ 1 & 0 & 0 & 0 \end{bmatrix}. \quad (27)$$

Fig. 8 shows the initial operating states of the isolated microgrid. The frequencies on the buses fluctuate within about ± 0.01 Hz, when the microgrid can be regarded as operating in the stable state. The generating power outputs of DGs are about 8 kW and 16 kW, respectively. The fixed loads and VPPs on each bus are about 8.2 kW and 7.8 kW, respectively. Five typical scenarios are carried out in this paper:

Scenario 1: The microgrid operates in a relatively stable state and a small load disturbance of 2 kW occurs on the bus-5. In this scenario, the DGs are regulated by the DCA to make the microgrid frequency return back to the stable state. VPPs do not participate in the regulation service, because DGs can deal with small disturbances by themselves to decrease the regulation impacts on users.

Scenario 2: Compared with the Scenario 1, a large load disturbance of 10 kW occurs on the bus-5 and two cases are compared. *Case 1:* Assuming there is no VPPs and the DGs are controlled by the DCA. *Case 2:* The DGs and VPPs are coordinately controlled by the proposed DCA and LCA, respectively.

Scenario 3: An accidental DG outage occurs on bus-6, where the microgrid suddenly loses the generating power output around 16 kW from PV3. In this scenario, the communication links among the remaining DGs in normal operating state are also changed. More seriously, the regulation capacity in the supply-side becomes less (i.e., four DGs are decreased to three DGs) compared with load disturbances in Scenarios 1 and 2. Two cases similar to Scenario 2 are implemented to test the applicability of the proposed method in contingency conditions.

Scenario 4: The uncertainty of the AC's response is analyzed in this scenario. similar to the Scenario 2, a large load disturbance of 10 kW is assumed to occur on the bus-5. The DGs and VPPs are coordinately controlled by the proposed DCA and LCA, respectively, while around 10% of ACs in VPPs may not successfully participate in the coordination control.

Scenario 5: The uncertainty of the PV's power output is analyzed in this scenario. It is assumed that a moving cloud influences the power output of the DG3, whose maximum available power output is decreased from 40 kW at the beginning (i.e., 0 s) to 35 kW at 1 s, 30 kW at 2 s, and 25 kW at 3 s with the movement of clouds. The DGs and VPPs are coordinately controlled by the proposed DCA and LCA, respectively.

The above models and methods are implemented using Matlab 2021b with an Intel Core i7-9700 CPU @3.00 GHz with 16.0 GB RAM.

5.2. Result analysis of small disturbance in Scenario 1

Fig. 9(a) shows the small load disturbance on the bus-5, which causes the decrease of the frequency. As shown in Fig. 9(c), the maximum deviation from the rated frequency 50 Hz is around 0.08 Hz. The regulation power outputs from DGs are shown in Fig. 9(b), where all the DGs increase their generating power to assist the microgrid to recover the balance state. DG2 and DG4 increase about 350 W, while DG1 and DG3 increase about 650 W. It means that a DG with a larger capacity will provide more regulation power to the microgrid, because the proposed DCA is designed to achieve a fair utilization of each DG. Furthermore, DG2 and DG3 are regulated faster and larger compared with DG1 and DG4, because the buses of DG2 and DG3 are closer to bus-5 in this microgrid topology. This closer distance leads to earlier and larger frequency deviations on the buses of DG2 and DG3. In addition, it can be seen from Fig. 9(d) that the average frequency deviation is returned to the stable state in a short time. Therefore, the proposed DCA can effectively deal with small load disturbances in the microgrid.

5.3. Result analysis of large disturbance in Scenario 2

Fig. 10(a) shows a large load disturbance of 10 kW occurs on the bus-5. In this scenario, there are two cases. Case 1 in Fig. 10 shows results without considering VPPs, while Case 2 in Fig. 11 shows results considering VPPs. First, as shown in Figs. 10(b) and 11(b), the large disturbance causes DGs to be regulated higher and larger compared with the results in Scenario 1 in Fig. 9(b). Moreover, the regulation power outputs of DGs in Case 1 are higher than that in Case 2, because some regulation capacities are provided by VPPs in Case 2, as shown in Fig. 11(a). In the three VPPs, VPP2 is regulated the most rapidly, because VPP2 is on bus-5 and the load disturbance occurs on the same bus, which leads to the frequency on bus-5 deviates from the rated value earlier and larger. VPP1 is regulated the most slowly, because the bus of VPP1 (i.e., bus-4) is the furthest to bus-5 in this microgrid topology compared with other VPPs.

The frequency deviations on each bus in the two cases are shown in Figs. 10(c) and 11(c), respectively. In Case 1, the maximum frequency deviations on bus-1, 5, 6, and 7 are around 0.25 Hz, and they are around 0.18 Hz on bus-2, 3 and 4. In Case 2, the maximum frequency deviations on all the buses are mitigated by VPPs, as shown in Table 2. The average frequency deviation curves in Figs. 10(d) and 11(d) can be compared to illustrate the effectiveness of VPPs more clearly. The maximum deviation of the average frequency curve is 0.20 Hz in Case 1, while it is decreased to 0.12 Hz in Case 2. The recovery time of the frequency deviation to be less than 0.05 Hz is 4.5 s in Case 1, while it is shortened to 0.2 s in Case 2. That is to say, the maximum frequency

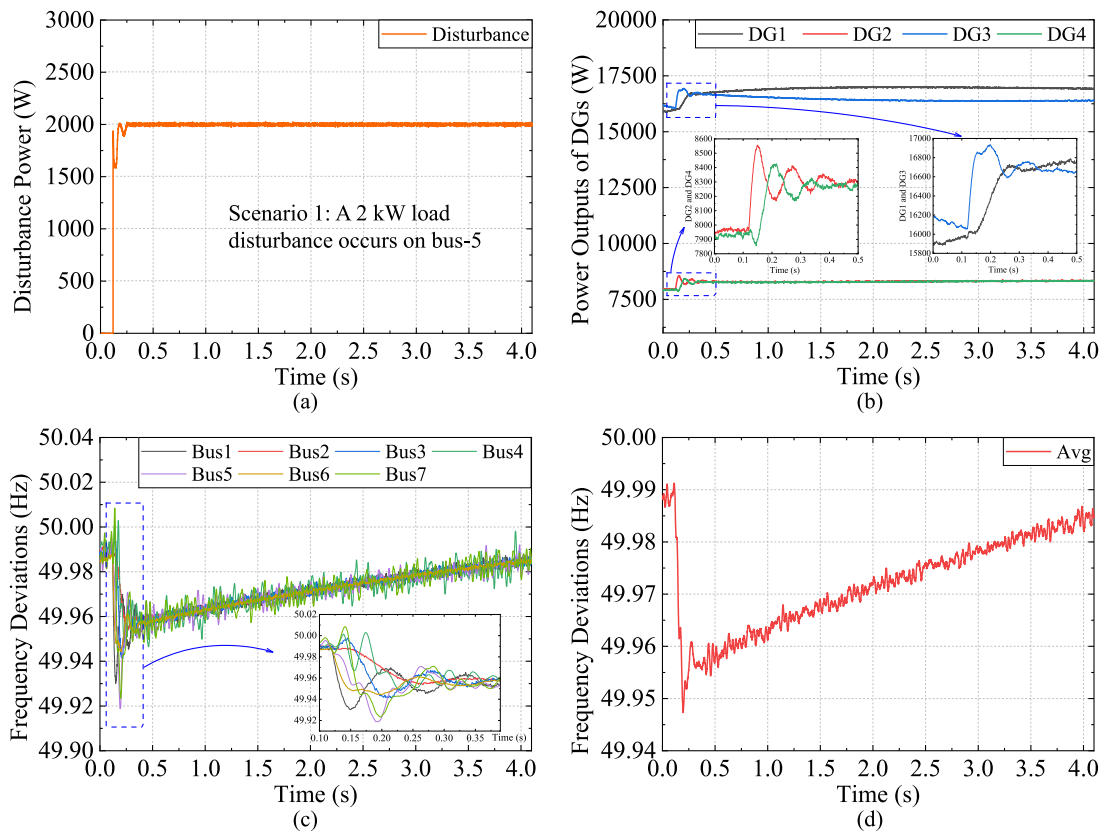


Fig. 9. The results in Scenario 1: (a) the disturbance power, (b) the generating power outputs of DGs, (c) the frequency deviations on buses, (d) the average frequency deviation of all the buses.

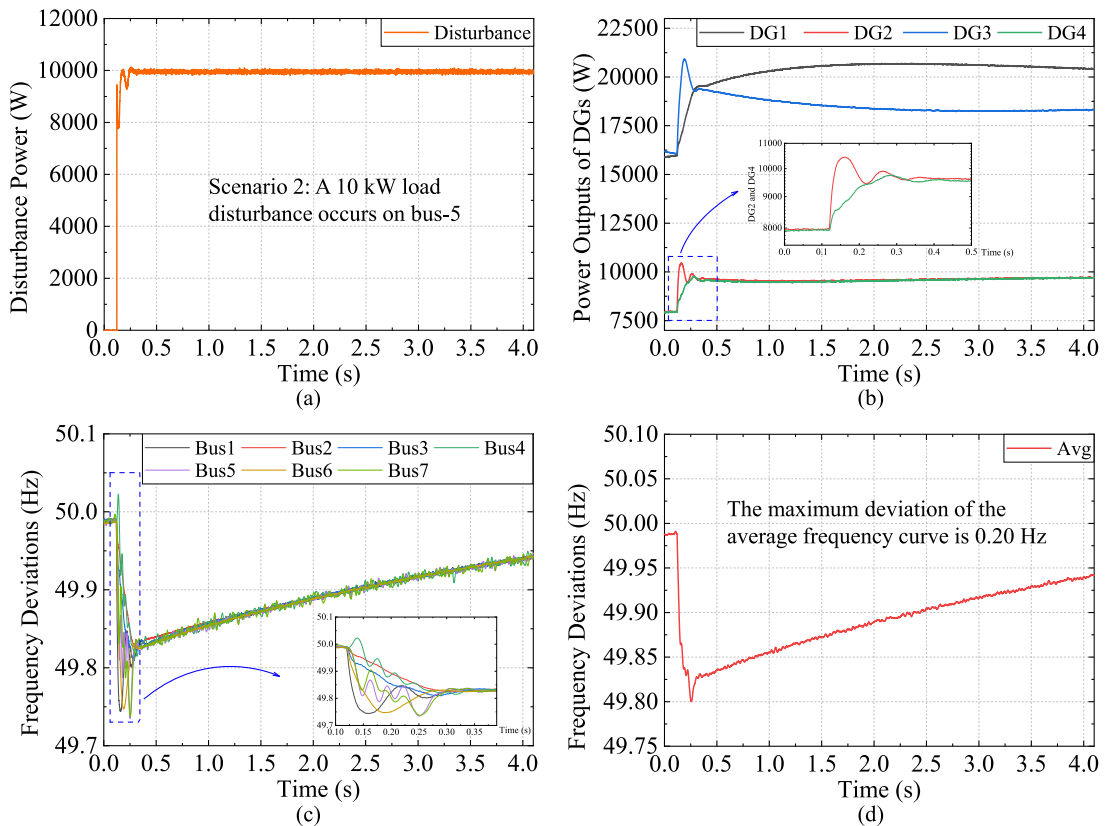


Fig. 10. The results in Scenario 2 (Case 1): (a) the disturbance power, (b) the generating power outputs of DGs, (c) the frequency deviations on buses, (d) the average frequency deviation of all the buses.

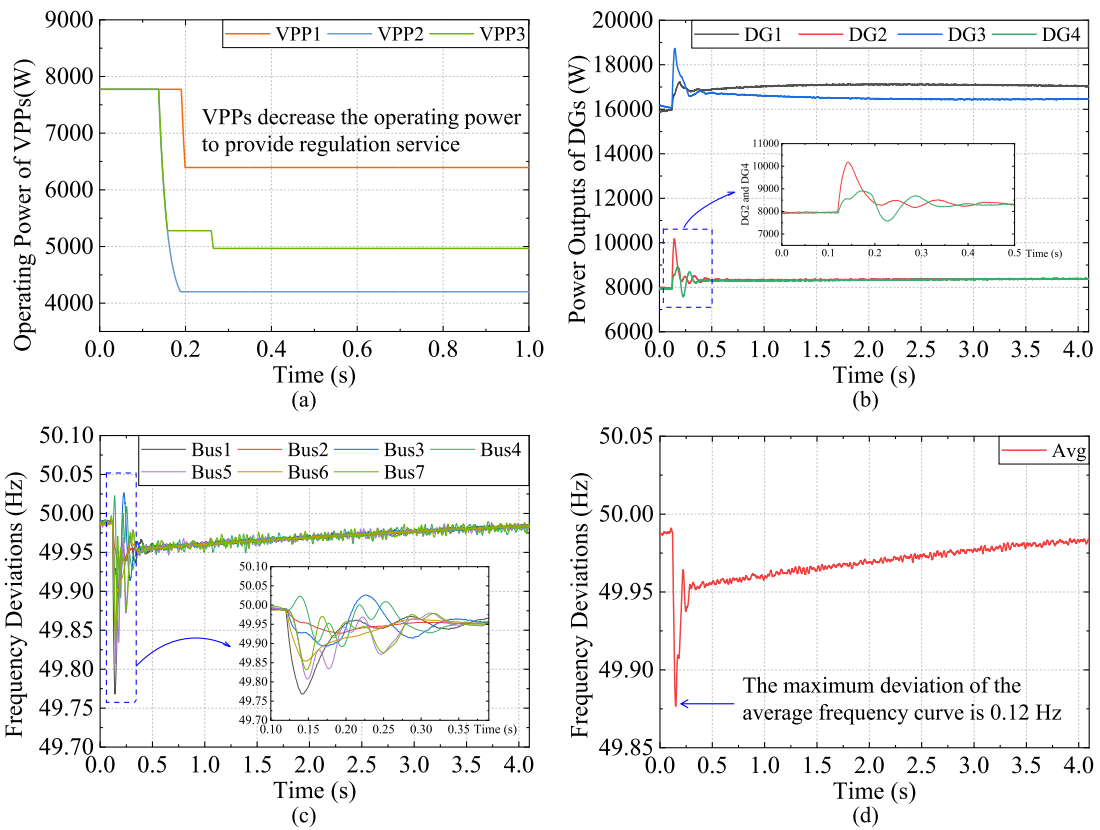


Fig. 11. The results in Scenario 2 (Case 2): (a) the operating power of VPPs, (b) the generating power outputs of DGs, (c) the frequency deviations on buses, (d) the average frequency deviation of all the buses.

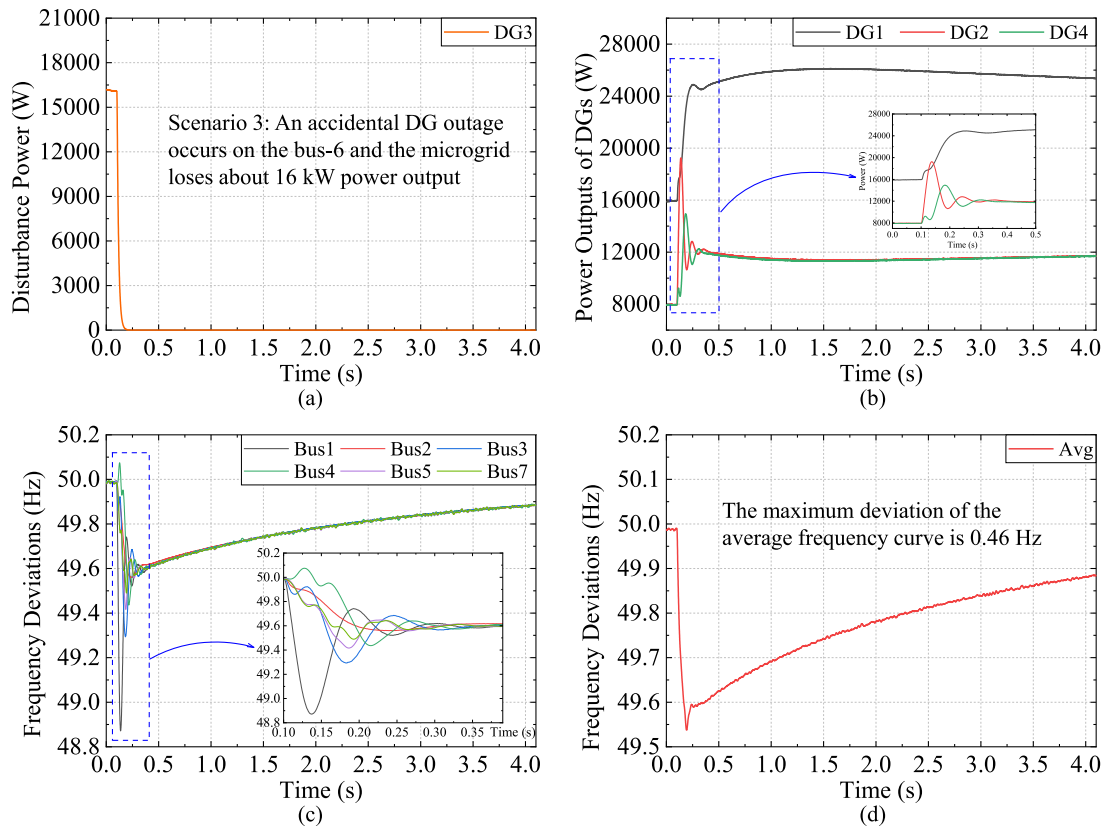


Fig. 12. The results in Scenario 3 (Case 1): (a) the disturbance power, (b) the generating power outputs of DGs, (c) the frequency deviations on buses, (d) the average frequency deviation of all the buses.

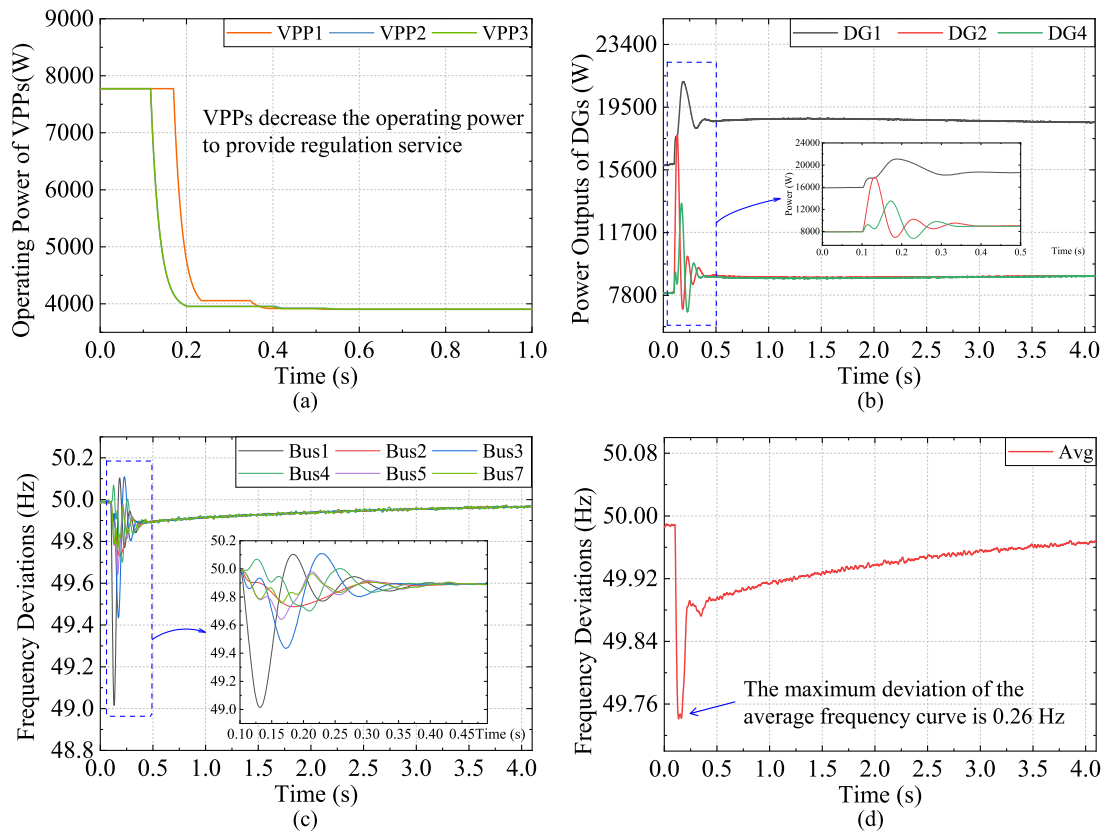


Fig. 13. The results in Scenario 3 (Case 2): (a) the operating power of VPPs, (b) the generating power outputs of DGs, (c) the frequency deviations on buses, (d) the average frequency deviation of all the buses.

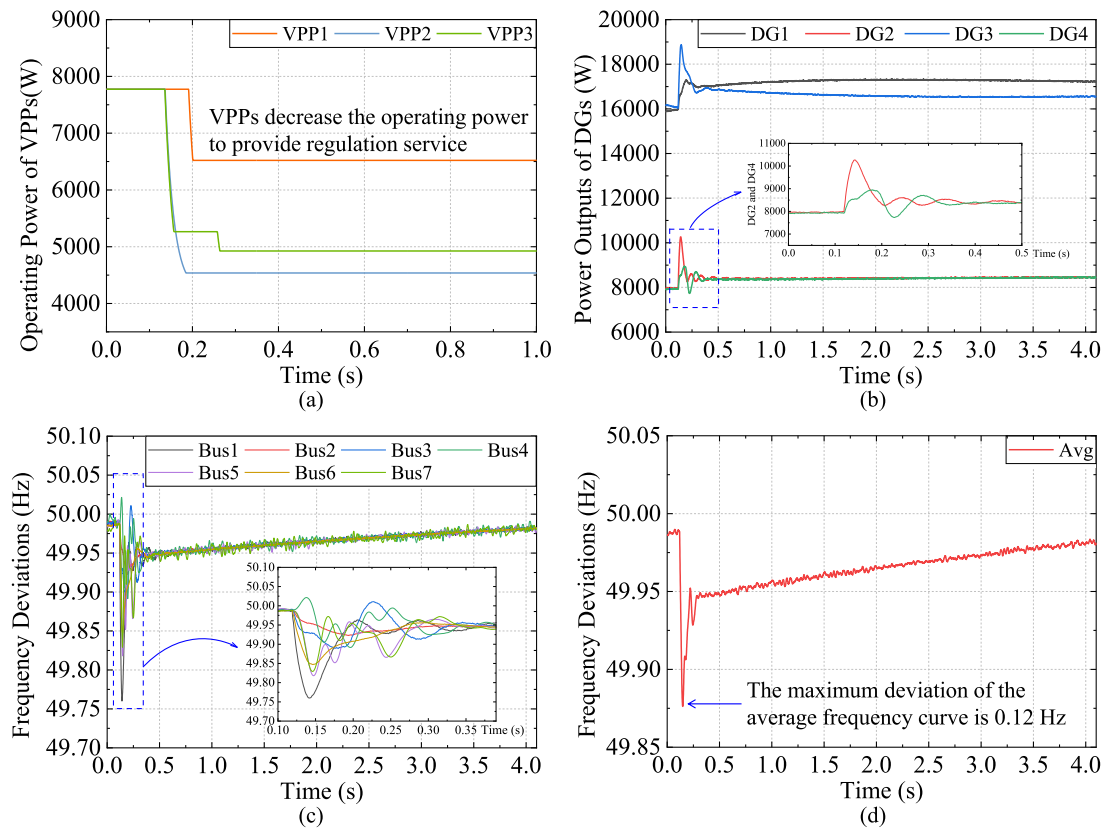


Fig. 14. The results in Scenario 4: (a) the operating power of VPPs, (b) the generating power outputs of DGs, (c) the frequency deviations on buses, (d) the average frequency deviation of all the buses.

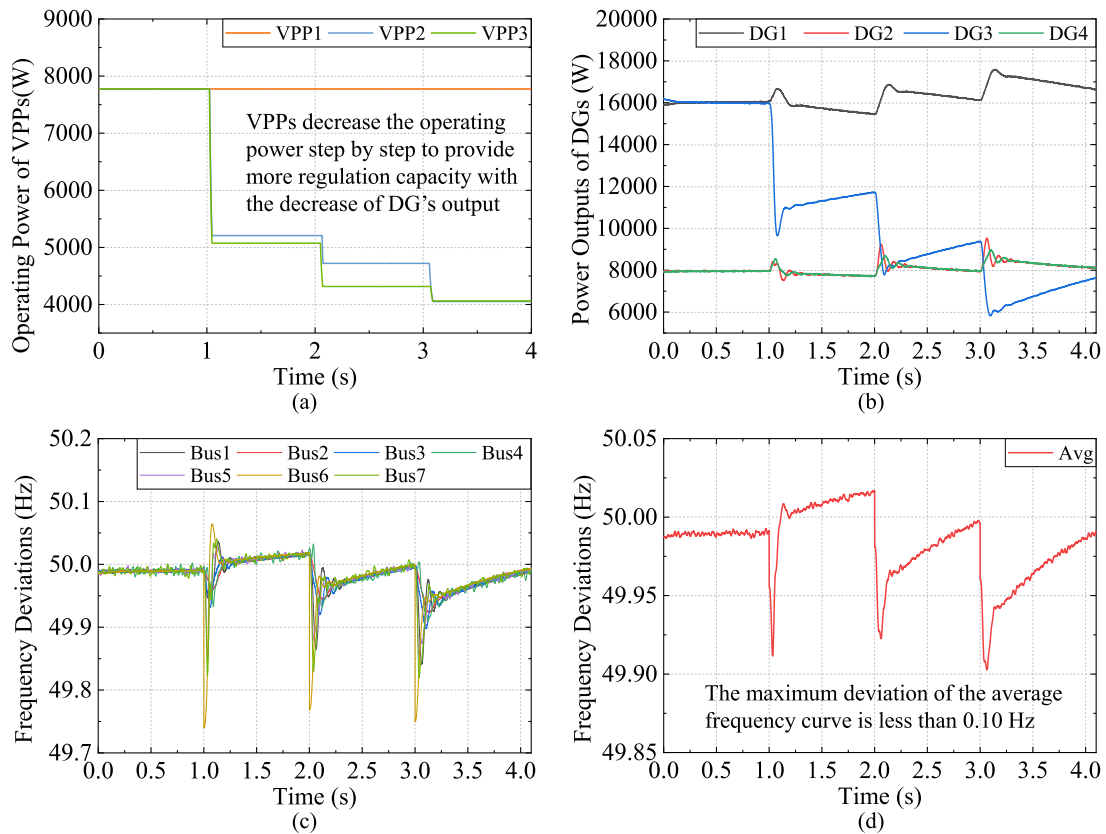


Fig. 15. The results in Scenario 5: (a) the operating power of VPPs, (b) the generating power outputs of DGs, (c) the frequency deviations on buses, (d) the average frequency deviation of all the buses.

deviation is reduced around 40%, and the recovery time is reduced around 95%. Therefore, the proposed coordination control framework considering VPPs can deal with large load disturbances effectively.

5.4. Result analysis of DG outage in Scenario 3

Fig. 12(a) shows an accidental DG outage on bus-6, where the microgrid loses the generating power output from PV3 suddenly, i.e., around 16 kW. In this scenario, the communication links among the remaining DGs in normal operating state are changed as follows:

$$\hat{A} = \begin{bmatrix} 0 & 1 & 0 & 1 \\ 1 & 0 & 0 & 0 \\ 0 & 0 & 0 & 0 \\ 1 & 0 & 0 & 0 \end{bmatrix}. \quad (28)$$

Compared with load disturbances in Scenarios 1 and 2, the DG outage causes the regulation capacity in the supply-side to become less. In this scenario, there are two cases. Case 1 in Fig. 12 shows the results without considering VPPs, while Case 2 in Fig. 13 shows the results considering VPPs. First, as shown in Figs. 12(b) and 13(b), the remaining DGs can still be regulated to provide regulation capacities for the microgrid. It proves that the proposed DCA is effective to control DGs in changeable communication links. Moreover, the regulation power outputs of DGs in Case 1 are higher than that in Case 2, because some regulation capacities are provided by VPPs in Case 2, as shown in Fig. 13(a). In the three VPPs, VPP2 and VPP3 are regulated more rapidly than VPP1, because VPP2 and VPP3 are on bus-5 and bus-7, respectively. These two buses are neighbors of the bus-6, which leads to the frequencies on bus-5 and bus-7 deviate from the rated value earlier and larger. VPP1 is regulated the most slowly, because the bus-4 is the furthest to bus-6 in this microgrid topology compared with other VPPs.

The frequency deviations on each bus in the two cases are shown in Figs. 12(c) and 13(c), respectively. In both Case 1 and Case 2, the

maximum frequency deviation is on bus-1, which is about 1.13 Hz and 0.99 Hz, respectively. Hence, VPPs contribute to improving the stability of the microgrid frequency. The average frequency deviation curves in Figs. 12(d) and 13(d) can be compared to illustrate the effectiveness of VPPs more clearly. The maximum deviation of the average frequency curve is 0.46 Hz in Case 1, while it is decreased to 0.26 Hz in Case 2. The recovery time of the frequency deviation to be less than 0.05 Hz is around 5.1 s in Case 1, while it is shortened to 2.9 s in Case 2. That is to say, the recovery time is reduced around 43%. It proves that the VPPs can effectively compensate for the shortage of regulation capacities caused by DG outages. Therefore, the proposed coordination control framework considering VPPs can play a significant role in accidental DG outages.

5.5. Result analysis of AC response uncertainty in Scenario 4

In this scenario, around 10% of ACs in VPPs may not successfully participate in the coordination control. The most direct influence is the decrease of regulation capacities from VPPs, as the comparison in Figs. 11(a) and 14(a). However, the influence on the system frequency deviations is little, as shown in Fig. 14(c), because the lost regulation capacities from VPPs can be supplemented by DGs in the microgrid. Therefore, the maximum deviation of the average frequency curve in Fig. 14(d) maintains 0.12 Hz, which is similar to the result in Fig. 11(d).

Note that the influence may be more serious with the increase of unsuccessful response ACs. To avoid this issue, in practical projects, the adjustable ACs are invited by the system operator in the day-ahead and the end-users should answer the invitation to decide whether participating in the regulation service. If some answers are no, these ACs will not be counted in the available regulation capacity. Then, the system operator has enough time to purchase and reserve other regulation resources. If some answers are yes in the day-ahead while they do not

Table 2
Regulation results of DGs and VPPs in the five scenarios.

Scenario and case	$\Delta f_{\text{Bus1}}^{\text{max}}$ (Hz)	$\Delta f_{\text{Bus2}}^{\text{max}}$ (Hz)	$\Delta f_{\text{Bus3}}^{\text{max}}$ (Hz)	$\Delta f_{\text{Bus4}}^{\text{max}}$ (Hz)	$\Delta f_{\text{Bus5}}^{\text{max}}$ (Hz)	$\Delta f_{\text{Bus6}}^{\text{max}}$ (Hz)	$\Delta f_{\text{Bus7}}^{\text{max}}$ (Hz)	$\Delta f_{\text{Avg}}^{\text{max}}$ (Hz)	Recovery time (s)
S1	0.070	0.046	0.059	0.053	0.081	0.056	0.077	0.053	≤0.1
S2-1	0.256	0.175	0.191	0.185	0.265	0.253	0.262	0.200	4.5
S2-2	0.232	0.074	0.107	0.108	0.193	0.146	0.168	0.123	0.2
S3-1	1.129	0.440	0.707	0.564	0.584	0.016	0.510	0.463	5.1
S3-2	0.985	0.270	0.566	0.299	0.359	0.016	0.241	0.259	2.9
S4	0.240	0.077	0.111	0.108	0.182	0.153	0.171	0.124	0.5
S5	0.159	0.077	0.102	0.090	0.152	0.260	0.180	0.097	≤0.3

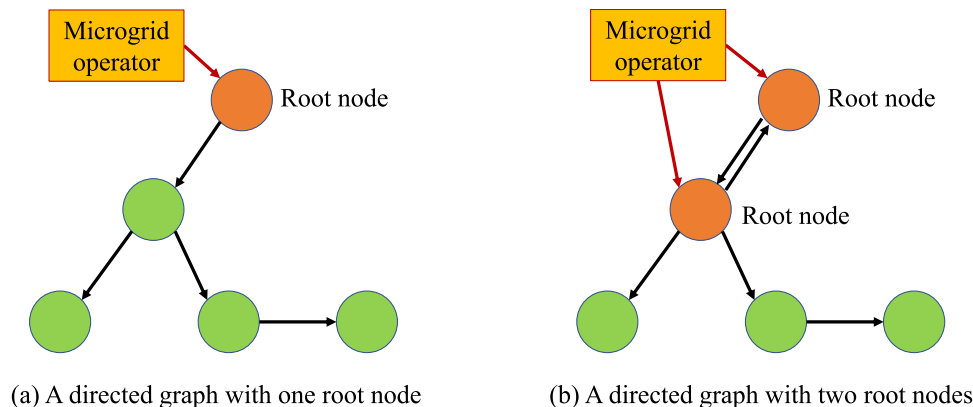


Fig. 16. The spanning tree for communication between the microgrid operator and DGs.

respond successfully in the real-time, these ACs will be punished. This manner can assist to decrease the proportion of unsuccessful response ACs. The above discussions are related to electricity market, while this paper mainly focuses on the effectiveness of the proposed control method. Scenario 4 verifies that the remaining ACs and DGs can still be regulated successfully even if some ACs may not participate in the coordination control.

5.6. Result analysis of DG output uncertainty in Scenario 5

In this scenario, it is assumed that a moving cloud influences the power output of the DG3. As shown in Fig. 15(b), the power output from the DG3 is decreased at 1 s, 2 s, and 3 s, while the other DGs increase the power outputs to supplement the lost capacities at the same time. The reason is that DGs are regulated by the proposed DCA, which is based on each DG's real-time maximum available power output to achieve the fair utilization of DGs. In addition, VPPs decrease the operating power step by step to provide more regulation capacity with the decrease of DG's power, as shown in Fig. 15(a). The VPP1 does not provide regulation capacity in this scenario, because the local frequency deviations on bus-4 do not reach the threshold $\Delta\omega_{\text{thr}}$ for participating in regulation services. The VPP2 on bus-5 and VPP3 on bus-7 are controlled to provide regulation capacities, because they are neighbors of the DG3 on bus-6 and get larger influences than VPP1 on bus-4. The Fig. 15(c) and (d) show that the system frequency deviations can be regulated near to the rated value. It illustrates that the proposed method can deal with the DG output uncertainties.

6. Conclusion

This paper proposes a coordination control method to tap flexibility in the isolated microgrid from both DGs in supply-side and load resources in demand-side. First, the microgrid model with high-penetration DGs is developed considering VPPs by aggregating ACs. Then, a coordination control framework is proposed for DGs and VPPs in multi-scenarios, including stable operation, uncertain load disturbances, and accidental DG outages. Then, a DCA and LCA are designed

for DGs and VPPs, respectively. Compared with traditional centralized control algorithms, the DCA can achieve a quick regulation of DGs with low communication requirement while good plug-and-play expansibility to deal with highly uncertain DGs. The LCA can fulfill the quality of regulation services for microgrids without compromising heterogeneous users' comfortable requirements. Finally, numerical studies verify that the maximum frequency deviation can be reduced around 40% from 0.20 Hz to 0.12 Hz faced with large load disturbances. The recovery time can be reduced around 43% in accidental DG outages. Therefore, the proposed methods can provide references for developing resilient isolated microgrids with high-penetration distributed renewable energies.

CRedit authorship contribution statement

Hongxun Hui: Conceptualization, Investigation, Methodology, Software, Validation, Writing – original draft, Writing – review & editing. **Yulin Chen:** Conceptualization, Investigation, Methodology, Software, Validation, Writing – original draft, Writing – review & editing. **Shaohua Yang:** Software, Validation, Data curation, Plot figures. **Hongcai Zhang:** Supervision, Project administration. **Tao Jiang:** Supervision, Project administration.

Declaration of competing interest

The authors declare that they have no known competing financial interests or personal relationships that could have appeared to influence the work reported in this paper.

Data availability

No data was used for the research described in the article.

Acknowledgments

This work is funded by the Science and Technology Development Fund, Macau SAR (File no. SKL-IOTSC(UM)-2021-2023, File no. 0003/2020/AKP).

Appendix. Discussion on the root node

In the distributed control, the communication network for the DGs is depicted and modeled as a directed graph. To achieve the global control objective, the communication network should be constructed into at least a spanning tree (A directed tree is a directed graph, where every node, except the root node, has exactly one parent. A spanning tree is a directed tree formed by graph edges that connect all the nodes of the directed graph). And the root DG should communicate with the microgrid operator. Therefore, for the distributed control in this paper, at least one DG (i.e., the root DG) should communicate with the microgrid operator. However, if the communication network contains more than one root node (i.e., more than one spanning tree, as shown in Fig. 16(b)), every root DG can be arranged to communicate with the microgrid operator. Thus, we can conclude that the number of DGs n_o that should communicate with the microgrid operator is $1 \leq n_o \leq N_r$, where N_r is the number of root nodes.

References

- [1] Energy, UN-habitat. 2022, [Online]. Available: <https://unhabitat.org/topic/energy>.
- [2] Renewables global status report, REN21. 2022, [Online]. Available: <https://www.ren21.net/reports/global-status-report>.
- [3] Chen Y, Li C, Qi D, Li Z, Wang Z, Zhang J. Distributed event-triggered secondary control for islanded microgrids with proper trigger condition checking period. *IEEE Trans Smart Grid* 2022;13(2):837–48.
- [4] Zheng M, Wang X, Meinrenken CJ, Ding Y. Economic and environmental benefits of coordinating dispatch among distributed electricity storage. *Appl Energy* 2018;210:842–55.
- [5] Wang H, Yan Z, Shahidehpour M, Zhou Q, Xu X. Optimal energy storage allocation for mitigating the unbalance in active distribution network via uncertainty quantification. *IEEE Trans Sustain Energy* 2020;12(1):303–13.
- [6] Zhou Q, Li Z, Wu Q, Shahidehpour M. Two-stage load shedding for secondary control in hierarchical operation of islanded microgrids. *IEEE Trans Smart Grid* 2019;10(3):3103–11.
- [7] Hui H, Siano P, Ding Y, Yu P, Song Y, Zhang H, Dai N. A transactive energy framework for inverter-based HVAC loads in a real-time local electricity market considering distributed energy resources. *IEEE Trans Ind Inf* 2022;18(12):8409–21.
- [8] Yan M, Shahidehpour M, Paaso A, Zhang L, Alabdulwahab A, Abusorrah A. Distribution network-constrained optimization of peer-to-peer transactive energy trading among multi-microgrids. *IEEE Trans Smart Grid* 2020;12(2):1033–47.
- [9] Siano P, Sarno D. Assessing the benefits of residential demand response in a real time distribution energy market. *Appl Energy* 2016;161:533–51.
- [10] Shi Q, Li F, Liu G, Shi D, Yi Z, Wang Z. Thermostatic load control for system frequency regulation considering daily demand profile and progressive recovery. *IEEE Trans Smart Grid* 2019;10(6):6259–70.
- [11] Hu J, Ye C, Ding Y, Tang Y, Liu S. A distributed MPC to exploit reactive power V2G for real-time voltage regulation in distribution networks. *IEEE Trans Smart Grid* 2021;13(1):576–88.
- [12] Zheng M, Meinrenken CJ, Lackner KS. Agent-based model for electricity consumption and storage to evaluate economic viability of tariff arbitrage for residential sector demand response. *Appl Energy* 2014;126:297–306.
- [13] Kim Y, Norford LK. Optimal use of thermal energy storage resources in commercial buildings through price-based demand response considering distribution network operation. *Appl Energy* 2017;193:308–24.
- [14] Hong J, Hui H, Zhang H, Dai N, Song Y. Distributed control of large-scale inverter air conditioners for providing operating reserve based on consensus with nonlinear protocol. *IEEE Internet Things J* 2022;9(17):15847–57.
- [15] Yan B, Long E, Meng X. Dynamic thermal reaction analysis of wall structures in various cooling operation conditions. *Energy Convers Manage* 2015;105:872–9.
- [16] Hui H, Ding Y, Luan K, Chen T, Song Y, Rahman S. Coupon-based demand response for consumers facing flat-rate retail pricing. *CSEE J Power Energy Syst* 2022;Early Access.
- [17] Zhang X, Pipattanasomporn M, Rahman S. A self-learning algorithm for coordinated control of rooftop units in small-and medium-sized commercial buildings. *Appl Energy* 2017;205:1034–49.
- [18] Zhou Q, Shahidehpour M, Paaso A, Bahramirad S, Alabdulwahab A, Abusorrah A. Distributed control and communication strategies in networked microgrids. *IEEE Commun Surv Tutor* 2020;22(4):2586–633.
- [19] Zhong H, Zhang G, Tan Z, Ruan G, Wang X. Hierarchical collaborative expansion planning for transmission and distribution networks considering transmission cost allocation. *Appl Energy* 2022;307:118147.
- [20] Wang J, Huang S, Wu D, Lu N. Operating a commercial building HVAC load as a virtual battery through airflow control. *IEEE Trans Sustain Energy* 2020;12(1):158–68.
- [21] Li Y, Wang Y, Chen Q. Study on the impacts of meteorological factors on distributed photovoltaic accommodation considering dynamic line parameters. *Appl Energy* 2020;259:114133.
- [22] Yu P, Hui H, Zhang H, Chen G, Song Y. District cooling system control for providing operating reserve based on safe deep reinforcement learning. 2021, arXiv preprint:2112.10949.
- [23] Deng Y, Jiang W, Hu F, Sun K, Yu J. Resilience-oriented dynamic distribution network with considering recovery ability of distributed resources. *IEEE J Emerg Sel Top Circuits Syst* 2022;12(1):149–60.
- [24] Gan W, Yan M, Yao W, Wen J. Peer to peer transactive energy for multiple energy hub with the penetration of high-level renewable energy. *Appl Energy* 2021;295:117027.
- [25] Li Z, Shahidehpour M, Aminifar F, Alabdulwahab A, Al-Turki Y. Networked microgrids for enhancing the power system resilience. *Proc IEEE* 2017;105(7):1289–310.
- [26] Hui H, Ding Y, Lin Z, Siano P, Song Y. Capacity allocation and optimal control of inverter air conditioners considering area control error in multi-area power systems. *IEEE Trans Power Syst* 2019;35(1):332–45.
- [27] Shi Q, Li F, Kuruganti T, Olama M, Dong J, Wang X, Winstead C. Resilience-oriented DG siting and sizing considering stochastic scenario reduction. *IEEE Trans Power Syst* 2020;36(4):3715–27.
- [28] Hui H, Ding Y, Zheng M. Equivalent modeling of inverter air conditioners for providing frequency regulation service. *IEEE Trans Ind Electron* 2018;66(2):1413–23.
- [29] Song M, Gao C, Yan H, Yang J. Thermal battery modeling of inverter air conditioning for demand response. *IEEE Trans Smart Grid* 2017;9(6):5522–34.
- [30] Zhang X, Biagioni D, Cai M, Graf P, Rahman S. An edge-cloud integrated solution for buildings demand response using reinforcement learning. *IEEE Trans Smart Grid* 2020;12(1):420–31.
- [31] Cai M, Pipattanasomporn M, Rahman S. Day-ahead building-level load forecasts using deep learning vs. traditional time-series techniques. *Appl Energy* 2019;236:1078–88.
- [32] Chen G, Zhang H, Hui H, Song Y. Fast Wasserstein-distance-based distributionally robust chance-constrained power dispatch for multi-zone HVAC systems. *IEEE Trans Smart Grid* 2021;12(5):4016–28.
- [33] Huang C, Zhang H, Song Y, Wang L, Ahmad T, Luo X. Demand response for industrial micro-grid considering photovoltaic power uncertainty and battery operational cost. *IEEE Trans Smart Grid* 2021;12(4):3043–55.
- [34] Jiang T, Li Z, Jin X, Chen H, Li X, Mu Y. Flexible operation of active distribution network using integrated smart buildings with heating, ventilation and air-conditioning systems. *Appl Energy* 2018;226:181–96.
- [35] Chen T, Cui Q, Gao C, Hu Q, Lai K, Yang J, Lyu R, Zhang H, Zhang J. Optimal demand response strategy of commercial building-based virtual power plant using reinforcement learning. *IET Gener Transm Distrib* 2021;15(16):2309–18.
- [36] Guerrero JM, Vasquez JC, Matas J, de Vicuna LG, Castilla M. Hierarchical control of droop-controlled AC and DC microgrids—A general approach toward standardization. *IEEE Trans Ind Electron* 2011;58(1):158–72.
- [37] Bidram A, Davoudi A. Hierarchical structure of microgrids control system. *IEEE Trans Smart Grid* 2012;3(4):1963–76.
- [38] Wang C. Analysis and simulation theory of microgrids. Beijing: Science Press; 2013.
- [39] Shi Q, Liu W, Zeng B, Hui H, Li F. Enhancing distribution system resilience against extreme weather events: Concept review, algorithm summary, and future vision. *Int J Electr Power Energy Syst* 2022;138:107860.
- [40] Xin H, Qu Z, Seuss J, Maknouninejad A. A self-organizing strategy for power flow control of photovoltaic generators in a distribution network. *IEEE Trans Power Syst* 2010;26(3):1462–73.
- [41] Xin H, Lu Z, Qu Z, Gan D, Qi D. Cooperative control strategy for multiple photovoltaic generators in distribution networks. *IET Control Theory Appl* 2011;5(14):1617–29.
- [42] Bidram A, Davoudi A, Lewis FL, Guerrero JM. Distributed cooperative secondary control of microgrids using feedback linearization. *IEEE Trans Power Syst* 2013;28(3):3462–70.
- [43] Chen Y, Qi D, Li Z. Distributed event-triggered control for frequency restoration in islanded microgrids with reduced trigger condition checking. *CSEE J Power Energy Syst* 2021;Early access.
- [44] Chen Y, Qi D, Dong H, Li C, Li Z, Zhang J. A FDI attack-resilient distributed secondary control strategy for islanded microgrids. *IEEE Trans Smart Grid* 2021;12(3):1929–38.
- [45] Bidram A, Davoudi A, Lewis FL. A multiobjective distributed control framework for islanded AC microgrids. *IEEE Trans Ind Inf* 2014;10(3):1785–98.
- [46] Olfati-Saber R, Fax JA, Murray RM. Consensus and cooperation in networked multi-agent systems. *Proc IEEE* 2007;95(1):215–33.

- [47] Chen Y, Qi D, Li Z, Wang Z, Zhang J, Yu M. Distributed cooperative control of microgrid under false data injection attacks. *Autom Electr Power Syst* 2021;45(05):97–103.
- [48] Shivakumar PN, Chew KH. A sufficient condition for nonvanishing of determinants. *Proc Amer Math Soc* 1974;43(01):63–8.
- [49] Cui W, Ding Y, Hui H, Lin Z, Du P, Song Y, Shao C. Evaluation and sequential dispatch of operating reserve provided by air conditioners considering lead-lag rebound effect. *IEEE Trans Power Syst* 2018;33(6):6935–50.
- [50] Lu N. An evaluation of the HVAC load potential for providing load balancing service. *IEEE Trans Smart Grid* 2012;3(3):1263–70.
- [51] Chen G, Zhang H, Hui H, Dai N, Song Y. Scheduling thermostatically controlled loads to provide regulation capacity based on a learning-based optimal power flow model. *IEEE Trans Sustain Energy* 2021;12(4):2459–70.